Available online at www.sciencedirect.com

SCIENCE DIRECT®

Lithos 82 (2005) 169–184

LITHOS

www.elsevier.com/locate/lithos

U–Pb zircon and monazite geochronology of Variscan magmatism related to syn-convergence extension in Central Northern Portugal

B. Valle Aguado[a,*], M.R. Azevedo[a], U. Schaltegger[b], J.R. Martínez Catalán[c], J. Nolan[d]

[a]*Departamento de Geociências, Universidade de Aveiro, 3810-193 Aveiro, Portugal*
[b]*Department of Mineralogy, University of Geneva, 1205 Geneva and Institute of Isotope Geology and Mineral Resources, Federal Institute of Technology ETH, 8092 Zurich, Switzerland*
[c]*Departamento de Geología, Universidad de Salamanca, 37008 Salamanca, Spain*
[d]*Imperial College, London SW7 2BP, UK*

Received 17 October 2003; accepted 25 October 2004
Available online 5 February 2005

Abstract

The Viseu area is located in the Central Iberian Zone of the Iberian Variscan Belt and hosts numerous post-thickening, collision-related granitoids intruded into upper and middle crustal levels. The present paper reports high precision U–Pb zircon and monazite ages for four plutons of the Viseu area: the syn-kinematic granitoids of Maceira (314±5 Ma), Casal Vasco (311±1 Ma) and Junqueira (307.8±0.7 Ma) and the late-kinematic biotite monzogranites of Cota (306±9 Ma). This points to a synchronous emplacement of the different syn-kinematic plutons shortly followed by the intrusion of the late-kinematic granites and shows that the Upper Carboniferous plutonism occurred within a short time span of ca. 10 million years.

The ascent of granite magmas took place after an extensional tectonic event (D_2) and is coeval with dextral and sinistral crustal-scale transcurrent shearing (D_3). Field and petrographical evidence suggest a narrow time-span between peak T metamorphic conditions and the intrusion of granitic melts which implies very fast uplift rates accommodated through active tectonic exhumation. Magma compositions evolve through time, reflecting an increasing involvement of mid-crustal sources and the underplating effect of an upwelling asthenospheric mantle at the base of a thinning and stretching continental crust.

Keywords: Iberian Variscan Belt; Exhumation; Extension; Transcurrent tectonics; Collision granites; U–Pb dating

1. Introduction

The Variscan Belt of Europe was formed during the complex and polycyclic collision of Laurentia–Baltica with Gondwana in the Devonian/Carboniferous. Terrane accretion played an important role in the formation of the belt. In the internal zones of the orogen, collisional tectonics was contemporaneous with and immediately followed by rapid exhumation of crystalline complexes, voluminous granitic intrusions and high temperature/low pressure metamorphism (e.g. Burg et al., 1994; Schulmann et al., 2002).

* Corresponding author.
E-mail address: baguado@geo.ua.pt (B. Valle Aguado).

0024-4937/$ - see front matter © 2005 Elsevier B.V. All rights reserved.
doi:10.1016/j.lithos.2004.12.012

Many authors accept the view that crustal thickening during the Variscan collision was probably modest compared to the Alpine and Himalayan collisions as reflected in the early syn-collisional regional metamorphism being more generally of a medium pressure Barrovian-type (e.g. Finger et al., 1997; Sylvester, 1998). Behrmann et al. (1991) suggested a maximum crustal thickeness of ≈50 km for the Variscides. In these circumstances, in-situ radiogenic heating should not produce extensive HT-LP metamorphism and melting (Thompson and Connoly, 1995). Instead, the HT metamorphism and granite genesis would require a large mantle heat source at the base of the crust caused by asthenospheric upwelling (Wickham and Oxburgh, 1987; Thompson and Connoly, 1995), following slab break-off (Davies and Von Blanckenburg, 1995) and lithospheric delamination (e.g. Black and Liégeois, 1993; Burg and Ford, 1997; Rey et al., 1997).

Unlike in the Himalayas, the Variscan highly peraluminous syn-kinematic granitoids are closely associated with large volumes of post-kinematic calc-alkaline granites resulting from interaction between crustal melts and mantle-derived magmas that may have been produced in the asthenosphere (Rottura et al., 1991; Finger et al., 1997). This provides additional evidence for a "high temperature" collision setting for the Variscides in which the nature of the heat source necessary to induce large scale dehydration melting is not purely crustal and involves mantle-derived heating of a normally thickened crust (<50 km) after lithospheric delamination (Sylvester, 1998).

This paper addresses these questions and combines precise U–Pb zircon and monazite dating with structural and metamorphic data from the Viseu area (Northern Portugal) to model the geodynamic scenario in this sector of the Iberian Variscides.

2. The Iberian Massif

The Viseu area is located in the Iberian Variscan Belt, between latitudes 40°34′N–41°05′N and longitudes 7°23′W–8°35′W Greenwich (Fig. 1). The Iberian Variscan Belt, also known as the Iberian Massif,

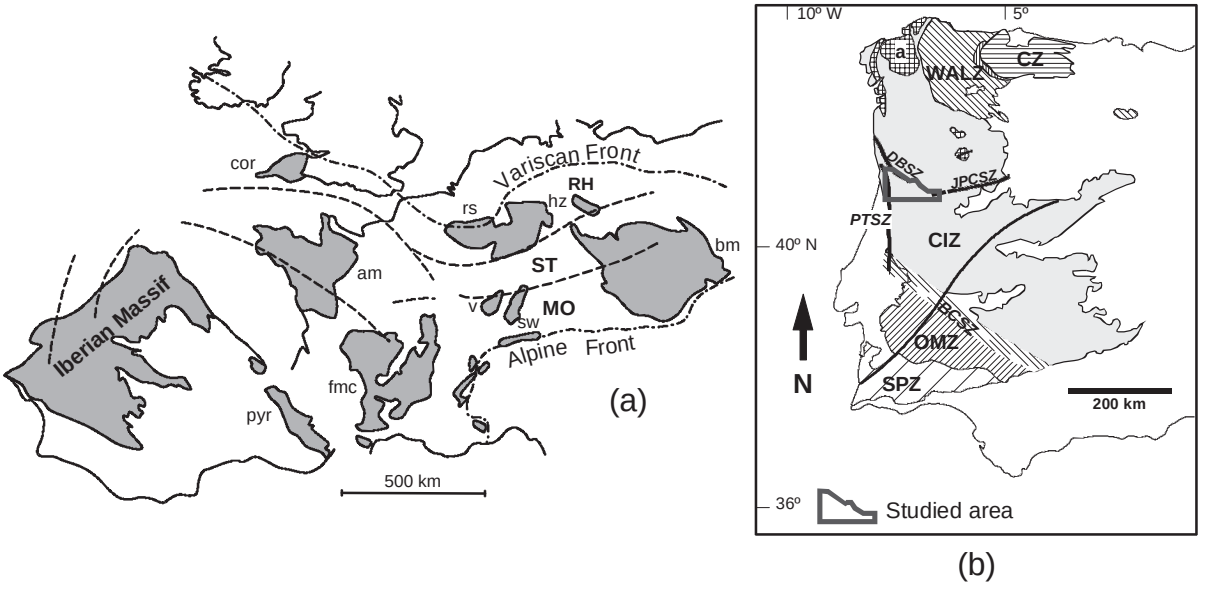

Fig. 1. (a) Structural subdivision of the Variscan Fold Belt showing the distribution of the major Variscan units of central Europe and Iberian Peninsula (after Behr et al., 1984). MO—Moldanubian Zone, RH—Renohercynian Zone, ST—Saxothuringian Zone. am—Armorican Massif, bm—Bohemian Massif, cor—Cornwall, fmc—French Massif Central, hz—Harz, pyr—Pyrenees, rs—Rheinisches Schiefergebirge, sw—Schwarzwald, v—Vosgues. (b) Subdivision in zones of the Iberian Massif (modified from Julivert et al., 1974): CIZ—Central Iberian Zone (a—allochthonous terrains), CZ—Cantabrian Zone, OMZ—Ossa–Morena Zone; SPZ—South Portuguese Zone; WALZ—West Asturian–Leonese Zone. *BCSZ*—Badajoz–Cordoba Shear Zone; *DBSZ*—Doro–Beira Shear Zone; *JPCSZ*—Juzbado–Penalva do Castelo Shear Zone; *PTSZ*—Porto–Tomar Shear Zone.

corresponds to the southwestern extension of the European Hercynides and constitutes one of the largest domains of the Variscan orogen that has escaped significant reworking by Alpine tectono-metamorphic events.

Julivert et al. (1972, 1974) subdivided the Iberian Massif into five main zones with different geological characteristics (Fig. 1b). These are, from NE to SW: the Cantabrian Zone (CZ); the West Asturian Leonese Zone (WALZ); the Central Iberian Zone (CIZ); the Ossa Morena Zone (OMZ) and the South Portuguese Zone (SPZ). More recently, Farias et al. (1987) included the allochthonous units of the CIZ in a separate zone called Galician Trás-os-Montes Zone (GTMZ), which occupies most of the northwestern sector of the Iberian Massif.

As shown in Fig. 1b, the study area is situated within the autochthonous terrains of the Central Iberian Zone. Lithostratigraphically, the CIZ is characterized by a) a clear predominance of Precambrian to Cambrian rocks, b) the absence of Middle and Upper Cambrian sequences and c) the transgressive nature of the Lower Ordovician quartzites (Arenig) (Díez Balda et al., 1990). The pre-Ordovician lithologies constitute a thick and monotonous megasequence of metapelites and greywackes, generally referred to as the "Complexo Xisto Grauváquico ante-Ordovícico" (CXG) (Carrington da Costa, 1950; Teixeira, 1954).

According to Dallmeyer et al. (1997) and Ábalos et al. (2002), Variscan crustal thickening started around 360 Ma in the CIZ autochthon, with the D_1 deformation phase inducing prograde metamorphism of Barrovian type. During the Early–Middle Carboniferous, the D_1 contractional structures were variably overprinted by a major D_2 extensional event attributed to a large-scale gravitational collapse of the thickened continental crust (e.g. Noronha et al., 1981; Escuder Viruete et al., 1994; Díez Balda et al., 1995; Valverde Vaquero, 1997; Ábalos et al., 2002).

Late stage D_3 deformation is related to strike-slip, sinistral and dextral, subvertical shear zones. It occurred under greenschist facies retrograde conditions at higher crustal levels whilst, in lower crustal levels, high temperatures could have locally persisted as a result of the high thermal gradients inherited from D_2 and the intrusion of synkinematic granitoids (Dallmeyer et al., 1997; Ábalos et al., 2002).

Huge volumes of granitic magmas represent, together with the migmatitic domes about 70% of the CIZ autochthon. Granite emplacement appears to postdate D_2 deformation and is predominantly correlated to the third Variscan deformation phase (D_3) (Ferreira et al., 1987; Pinto et al., 1987; Dias et al., 1998).

3. Tectono-metamorphic framework of the Viseu area

Most of the Viseu area is occupied by Hercynian granitoids intruded into two major metamorphic complexes (Fig. 2): a) the Porto–Sátão Syncline, produced by the first Hercynian deformational event (D_1) and subsequently affected by D_3 deformation and b) the Porto–Viseu Belt, corresponding to a megascopic antiformal structure developed during D_3.

The Porto–Viseu Belt is composed of pelitic rocks interbedded with greywackes and relatively thin calc-silicate layers of the CXG and constitutes a classical example of a gneiss dome with medium- to high grade metasediments, HT-LP migmatites and anatectic syn-D_3 granites in the core and low- to very low-grade metasediments in the limbs.

The post-Cambrian Palaeozoic stratigraphic record is exposed in the core of the Porto–Sátão Syncline and includes a succession of Ordovician, Silurian, Lower Devonian and Upper Carboniferous deposits (Fig. 2). These megasequences can be grouped into two main units: a) the pre-orogenic to syn-orogenic materials of Lower Ordovician to Lower Devonian age and b) the post-orogenic Upper Carboniferous unmetamorphosed, continental, coal-bearing deposits formed in a narrow intramontane limnic tectonic basin. This basin is limited by a reverse fault in the northeast and an unconformity in the southwest.

3.1. Tectonic setting

The tectonic evolution of the Viseu area has been explained in terms of the superposition of the three consecutive Variscan deformation phases D_1, D_2 and D_3 (Valle Aguado, 1992; Valle Aguado et al., 2000). The earlier D_1 deformation phase has affected all the pre-Carboniferous sedimentary sequences and produced NW–SE subvertical folds with an axial planar

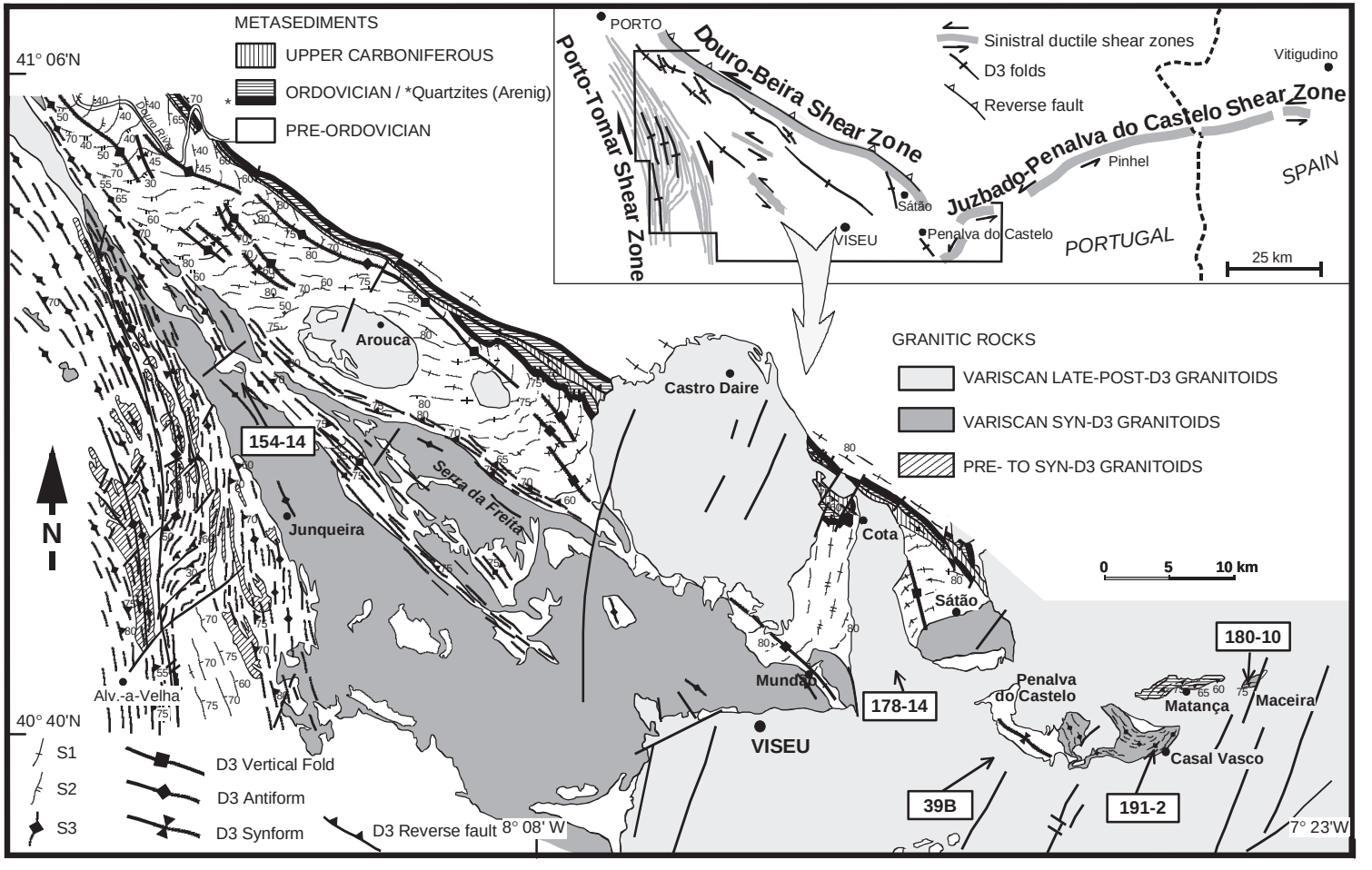

Fig. 2. Simplified geological map and tectonic setting of the Viseu region. U–Pb sample locations are shown.

slaty cleavage or schistosity (S_1). The strike of the main D_1-structures was subsequently modified by later (particularly D_3) folding events and/or shearing.

D_2 is characterized by heterogeneous ductile deformation and affects mainly the medium- to high-grade metamorphic CXG lithologies of the Porto–Viseu Belt. It produced subhorizontal minor folds with a crenulation axial–planar S_2 fabric. As discussed below, the variation of *P–T* conditions during D_2 is imprinted on the mineral assemblages related to the S_2 fabrics and provides strong evidence in favour of an extensional character for this tectonometamorphic event (Valle Aguado, 1992; Valle Aguado et al., 1993).

The third deformation phase (D_3) is responsible for the refolding of both the D_1+D_2 structures and the metamorphic isograds. It produced asymmetric, kilometric-scale subvertical folds with NW–SE to NNW–SSE trending axial planes and an en échelon arrangement in map view (Fig. 2). D_3 folds commonly show a poorly developed axial planar crenulation cleavage and vertical or steeply plunging (>65°) axes. In places where the pre-D_3 planar fabric is the S_2 schistosity, the fold axes may plunge gently to the SE.

In the study area, the D_3 deformation phase is related to three crustal-scale transcurrent shear zones (Fig. 2): the Porto–Tomar dextral shear zone (PTSZ), the Douro–Beira sinistral shear zone (DBSZ) and the sinistral Juzbado–Penalva do Castelo shear zone (JPCSZ) (Ribeiro et al., 1980, 1990; Iglesias and Ribeiro, 1981; Valle Aguado, 1992; Dias, 1994). It is generally agreed that these three shear zones have accommodated part of the shortening related to the final stages of the continental collision.

The ductile PTSZ shearing produced a very wide, NNW–SSE trending, high-strain shear zone in the western part of the Porto–Viseu Belt (Fig. 2). The DBSZ affected all the sequences exposed in the Porto–Sátão Syncline, including the Upper Carboniferous detrital succession. As a result, a NW–SE striking, penetrative, sub-vertical S_3 cleavage developed in the Pre-Carboniferous rocks. The DBSZ-related foliation is the only tectonic fabric recorded in the Upper Carboniferous sequence, suggesting that the formation of the intramontane limnic basin occurred prior to the transpressional stage, either at the end of D_2 crustal extension or in a transitional transtensional regime. Continued tectonic activity gave rise to basin inversion during late D_3 transcurrent tectonics.

The orientation of the Porto–Sátão syncline (NW–SE) changes to a N70E to E–W direction in the central part of the study area (Fig. 2). According to Iglesias and Ribeiro (1981), the sigmoidal curvature defined by the D_1-structures within this syncline documents the operation of the ENE–WNW striking, sinistral, ductile JPCSZ shear zone. In the western sector of the area there is no evidence of the JPCSZ. However, the presence of megascopic folds with anticlockwise asymmetry and sinistral NW–SE shear zones in this domain strongly suggests that the DBSZ may represent the western termination of the Juzbado–Penalva do Castelo sinistral shear system (Valle Aguado et al., 2000).

According to this interpretation, the JPCSZ continues through the NW–SE striking DBSZ which, due to its attitude, oblique to the main shear zone, had its motion partitioned into sinistral wrenching and reverse components. The former would have been accommodated by the NW–SE folding and by ductile shearing on the DBSZ and subsidiary sinistral shear zones. The latter was absorbed by the reverse fault which bounds the Carboniferous sediments to the north.

3.2. Metamorphic evolution

The metamorphic sequences of the Viseu area show no evidence of any pre-Variscan metamorphism. The Variscan regional metamorphism is recorded in the CXG metapelites of the Porto–Viseu Belt by a clear prograde metamorphic zoning characterized by a rapid increase of metamorphic grade from the chlorite and biotite zones to the staurolite, sillimanite and sillimanite+K-feldspar zones.

The typical mineral assemblages in the amphibolite and upper amphibolite grade schists consist of: a) biotite+quartz+plagioclase+staurolite±garnet± andalusite (retrograde)+muscovite and b) biotite+ quartz+plagioclase+fibrolite (±prismatic sillimanite)± staurolite (relict)±garnet (relict)±kyanite (relict)+ andalusite (retrograde)+muscovite. Microstructural criteria indicate that the growth of staurolite, garnet and kyanite is essentially syn-kinematic with D_1 structures, whilst the first appearance of sillimanite occurred early in relation to D_2 (Valle Aguado et al.,

1993). Some relict staurolite porphyroblasts are rimmed by coronas of andalusite+biotite. Andalusite also occurs as large syn-D_3 crystals containing abundant inclusions of all groundmass phases (including kyanite and sillimanite). The transition from initial intermediate pressure metamorphic conditions (Barrovian type) to a HT-LP regime provides evidence for a decompressive regional metamorphic episode during D_2.

The migmatites consist of biotite–sillimanite rich melanosomes interlayered with evenly spaced, foliation parallel, leucocratic domains composed by quartz+K-feldspar+plagioclase±sillimanite+muscovite (retrograde). The migmatite leucosomes are intensely deformed and folded. This folding is clearly correlated to the D_3 dextral and sinistral transcurrent shear zones and indicates that anatexis should have started before the D_3 deformation episode.

Based on the observed mineral assemblages and reaction textures, Valle Aguado et al. (1993) constrained the conditions of peak metamorphism for pelitic rocks of different crustal levels in the Porto–Viseu belt (Fig. 3). The inferred clockwise *P–T* path reflects burial and heating during crustal thickening (D_1), followed by decompression (D_2) and nearly isobaric cooling (D_3). For the deeper path, anatexis is expected to have occurred during the D_2 deformation

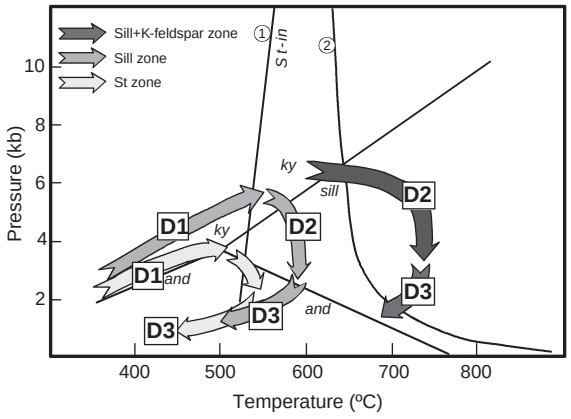

Fig. 3. Metamorphic *P–T* paths and relation with the major Variscan deformation phases (D_1, D_2 and D_3) for pelitic sequences of the Porto–Viseu belt (modified from Valle Aguado et al., 1993). *and*—andalusite; *ky*—kyanite; *sill*—sillimanite; *st*—staurolite; 1—"staurolite-in" curve (Yardley, 1989); 2—H_2O-saturated pelite solidus (Luth et al., 1964); phase diagram for Al_2SiO_5 polymorphs (Holdaway, 1971).

event and to have continued throughout the D_3 deformation episode. The widespread occurrence of migmatites in the core of the Porto–Viseu D_3 antiform suggests a temporal link between partial melting and exhumation.

The timing of the metamorphic climax is unknown. However, structural relationships show that the intrusion of the syn-D_3 peraluminous two-mica granites along the axial zone of the Porto–Viseu Belt post-dates the HT-LP metamorphic climax. In fact, these granites crosscut the high-grade metamorphic isograds and show evidence of heterogeneous deformation related to D_3. The available Rb–Sr isotopic ages for these granites vary from 326±4 Ma to 315±4 Ma (Reavy, 1987; Priem et al., 1984, respectively). Given the discrepancy of Rb–Sr ages obtained in these granites, it is fundamental to use isotopic dating methods less sensitive to temperature and/or deformation.

4. Granitic rocks

The Variscan granitoids of the Viseu area can be broadly grouped into three suites, according to geochemical, petrographical and tectonic criteria: a) the early, syn-D_3 granodiorite–monzogranite suite; b) the peraluminous leucogranite syn-D_3 suite and c) the late-post-D_3 granodiorite–monzogranite suite.

The early, syn-D_3 granodiorite–monzogranite suite is represented by two small intrusive bodies: the Maceira and Casal Vasco granites (Fig. 2). The syn-D_3 peraluminous two-mica granitoids constitute a large batholith elongated parallel to the D_3 structures (NW–SE), known as the Junqueira–Serra da Freita massif. Finally, the different facies of the late- to post-D_3 granodiorite–monzogranite suite occupy most of the central and eastern sectors of the Viseu area and include the Cota–Viseu coarse porphyritic biotite granites, several intrusions of two-mica granitoids and minor bodies of gabbros, monzodiorites, quartz monzodiorites and granodiorites.

5. Sampling and analytical techniques

Major-, trace- and rare-earth element data for selected samples of the three granite series are

Table 1
Major, trace and REE element compositions of representative samples of the Variscan granitoids from the Viseu area

	Syn-D_3 granodiorite–monzogranite suite				Syn-D_3 peraluminous granite suite		Late-post-D_3 granodiorite–monzogranite suite										
	Maceira granodiorites		C. Vasco monzogranites		Junqueira two-mica granites		Gabbros		Quartz monzodiorites		Cota–Viseu porphyritic biotite monzogranites					Two-mica granites	
Samples	180-9	180-10	190-36	191-2	154-13	154-9	188-8	188-4	190-2	190-3	11	37	39	178	178-14	130	9
SiO_2	60.84	66.17	70.95	70.04	71.84	73.49	52.64	52.94	60.84	60.07	70.35	67.66	69.78	71.39	69.51	72.97	75.84
TiO_2	1.20	0.80	0.45	0.57	0.19	0.13	0.56	0.73	1.33	1.00	0.75	0.61	0.63	0.36	0.53	0.22	0.07
Al_2O_3	16.45	15.75	14.77	15.39	14.60	15.47	18.49	18.26	15.85	17.08	13.45	15.05	14.29	14.29	14.63	14.09	14.10
Fe_2O_3 t	6.67	4.61	2.51	3.06	1.24	0.75	5.91	6.54	6.79	6.42	4.75	3.96	4.00	2.27	3.36	1.83	0.80
MnO	0.09	0.06	0.05	0.04	0.01	0.01	0.11	0.11	0.12	0.09	0.07	0.06	0.06	0.04	0.05	0.04	0.04
MgO	1.84	1.39	0.63	0.87	0.36	0.27	7.31	6.68	2.28	2.08	1.20	0.99	1.01	0.55	0.86	0.37	0.14
CaO	3.10	1.99	1.08	1.24	0.50	0.38	11.02	10.00	4.57	5.32	2.33	2.28	2.10	1.24	1.77	0.78	0.55
Na_2O	3.13	3.18	3.25	2.69	3.43	3.41	2.82	3.07	3.87	3.98	3.23	3.66	3.33	3.35	3.41	3.29	3.72
K_2O	5.10	5.10	5.20	4.84	5.63	4.49	0.55	0.79	3.29	2.98	3.25	4.20	4.27	4.78	5.06	5.02	4.48
P_2O_5	0.76	0.39	0.39	0.43	0.38	0.44	0.09	0.13	0.34	0.27	0.30	0.25	0.26	0.24	0.22	0.24	0.18
LOI	0.72	0.72	0.86	1.23	0.74	1.49	0.97	0.99	0.52	0.72	0.46	0.41	0.46	0.56	0.42	0.72	0.64
Total	99.90	100.16	100.14	100.40	98.92	100.47	99.80	100.24	99.80	100.01	100.14	99.13	100.19	99.07	99.82	99.57	100.56
Ba	2670	950	410	549	220	260	190	250	530	495	285	515	465	365	490	275	75
Rb	192	258	431	296	249	187	23	30	165	140	232	234	258	304	254	342	412
Sr	495	235	111	150	40	40	550	535	250	285	115	150	130	85	120	60	30
Zr	220	400	232	268	65	70	60	95	285	250	230	210	250	160	225	110	20
La	142.3	147.2	nd	102.3	nd	6.6	nd	14.2	38.8	nd	52.1	nd	nd	30.3	nd	27.5	5.1
Ce	290.3	322.2	nd	240.0	nd	14.3	nd	30.6	90.0	nd	112.9	nd	nd	66.0	nd	62.8	10.8
Pr	30.2	34.7	Nd	27.3	nd	1.3	nd	3.7	11.1	nd	13.2	nd	nd	7.8	nd	7.6	1.2
Nd	115.9	133.4	nd	106.1	nd	6.2	nd	15.0	46.2	nd	49.5	nd	nd	29.5	nd	28.7	4.5
Sm	17.8	19.9	nd	17.5	nd	1.8	nd	3.2	10.6	nd	10.5	nd	nd	6.3	nd	6.5	1.3
Eu	3.29	1.65	nd	1.2	nd	0.37	nd	1.01	1.85	nd	0.87	nd	nd	0.70	nd	0.40	0.17
Gd	11.23	10.48	nd	9.3	nd	1.82	nd	2.94	9.49	nd	8.85	nd	nd	5.14	nd	5.34	1.28
Dy	6.77	5.80	nd	4.2	nd	1.46	nd	2.76	8.66	nd	8.45	nd	nd	4.33	nd	4.79	1.73
Ho	1.29	1.13	nd	0.79	nd	0.20	nd	0.57	1.72	nd	1.68	nd	nd	0.79	nd	0.87	0.32
Er	3.46	2.85	nd	1.8	nd	0.54	nd	1.59	4.61	nd	5.21	nd	nd	2.30	nd	2.34	0.99
Yb	2.78	2.47	nd	1.5	nd	0.50	nd	1.48	4.07	nd	4.69	nd	nd	2.16	nd	2.11	1.02
Lu	0.39	0.35	nd	0.22	nd	0.07	nd	0.22	0.58	nd	0.64	nd	nd	0.31	nd	0.27	0.19

nd: not determined.

presented in Table 1. The Rb–Sr and Sm–Nd isotopic results for representative samples of the different granite units are listed in Table 2.

The whole rock compositions were determined at the University of London Imperial College (IC) by inductively coupled plasma atomic emission (ICP-AES). Subsets of these samples have been analysed for REE at the University of London Royal Holloway and Bedford New College (RHBNC) using cation exchange separation and ICP-AES (Watkins and Nolan, 1990, 1992). Analytical errors are less than 5% for most elements.

Isotopic analysis of Sr and Nd for the Cota–Viseu granites were performed on a VG 354 multicollector thermal ionization mass spectrometer at RHBNC. The remaining Sr and Nd isotopic analyses were obtained on a VG 354 multicollector thermal ionization mass spectrometer at the Centro de Pesquizas Geocronológicas of the University of São Paulo (Brasil). Rb and Sr were determined by XRF. Sm and Nd were determined by ID using the chemical separation technique described by Shaw (1991). The analytical data were corrected for mass fractionation using a linear law for Sr ($^{86}Sr/^{88}Sr$=0.1194) and an exponential law for Nd ($^{146}Nd/^{144}Nd$=0.7219; Thirlwall, 1991). Average levels of blanks were in the range 0.25–1.0 ng for Sr and 0.1–0.5 ng for Nd and Sm. The average values for standards measured in the period of analyses were 0.710247±2 (2 S.D. of 33 analyses) for SRM 987 standard at RHBNC and 0.71026±2 for NBS-987, at Centro de Pesquizas Geocronológicas of the University of São Paulo.

Zircon and monazite fractions from samples 180-10 (Maceira), 191-2 (Casal Vasco), 154-14 (Junqueira), 39B and 178-14 (Cota–Viseu) were used to determine the U–Pb ages. The location of these samples is shown in Fig. 2. Their petrographical characteristics are discussed in Section 6 and briefly summarized in Tables 3 and 4.

Zircon and monazite have been dated using conventional isotopic dilution techniques on single-grain or small multigrain fractions at ETH, Zurich and CRPG, Nancy. After crushing, the minerals were separated using standard heavy liquid and magnetic separation techniques. The bulk zircon fraction or non-magnetic zircon fraction was examined under binocular microscope. The selection of suitable zircon fractions was based mostly on morphological criteria and colour. Only transparent non-magnetic zircons, devoid of cracks and inclusions were selected for analysis. Air abrasion was applied to both zircon and monazite to remove zones of marginal lead loss (Krogh, 1982). The zircons were spiked with a mixed ^{205}Pb–^{235}U tracer prior to dissolution. Dissolution and chemical extraction followed the standard procedure developed by Krogh (1973), using miniaturized bombs and anion exchange columns. Total procedural blanks were continuously monitored yielding values around 2 ± 1 pg Pb and 0.1 pg U (ETH) and 26–94 pg Pb (CRPG). Isotopic measurements on samples

Table 2
Sr and Nd isotopic data for selected samples of the Variscan granitoids from the Viseu area

Sample	Location	Rock type	Rb	Sr	$^{87}Rb/^{86}Sr$	$^{87}Sr/^{86}Sr$	$^{87}Sr/^{86}Sr_i$	Sm	Nd	$^{147}Sm/^{144}Nd$	$^{143}Nd/^{144}Nd$	εNd_i
Syn-D_3 granodiorite–monzogranite suite												
180-9	Maceira	granodiorite	200.2	538.4	1.077	0.71205±9	0.707299	17.93	117.80	0.0920	0.512248±40	−3.47
180-10	Maceira	granodiorite	264.7	249.6	3.074	0.72294±9	0.709378	20.54	138.72	0.0895	0.512109±20	−6.08
190-36	C. Vasco	monzogranite	454.7	114.3	11.572	0.759153±13	0.708101	17.92	107.32	0.1010	0.512089±9	−6.93
Syn-D_3 peraluminous granite suite												
154-13	Junqueira	two-mica gr.	250.0	42.3	17.25	0.794295±24	0.718189	–	–	–	–	–
Late-post-D_3 granodiorite–monzogranite suite												
188-4	Viseu	gabbro	27.9	576.7	0.140	0.704730±10	0.704122	3.17	15.0	0.1275	0.512531±8	+0.61
190-3	Viseu	monzodiorite	140.4	304.0	1.337	0.710800±11	0.704997	6.91	33.30	0.1255	0.512499±21	+0.07
11	Cota–Viseu	monzogranite	213.1	120.2	5.122	0.729356±17	0.707125	9.08	43.46	0.1264	0.512503±45	+0.11
37	Cota–Viseu	monzogranite	230.4	151.5	4.492	0.724920±24	0.705858	6.93	33.33	0.1257	0.512396±6	−1.95
178	Cota–Viseu	monzogranite	308.3	76.9	11.615	0.758282±11	0.707867	6.03	29.39	0.1240	0.512313±7	−3.51

Table 3
U–Pb isotopic data on zircon and monazite from syn-D_3 granitoids

Number	Description[a]	Weight (mg)	No. of grains	Concentrations			Th/U[b]	Atomic ratios							Apparent ages			Error corr.
				U	Pb rad. (ppm)	Pb nonrad. (pg)		206/204[c]	206/238[d,e]	Error 2σ (%)	207/235[d]	Error 2σ (%)	207/206[d,e]	Error 2σ (%)	206/238	207/235	207/206	
180-10	*Maceira granite (deformed granitoid sample with a penetrative D_3 related foliation)*																	
1	z, lpr euh	0.0028	3	564	27.36	4.8	0.27	1038	0.04949	0.38	0.3594	0.58	0.05267	0.43	311.4	311.8	314.5	0.67
2	z, tips of lpr	0.0034	5	701	35.59	23.9	0.42	332	0.04966	0.41	0.3612	1.10	0.05276	0.98	312.4	313.1	318.3	0.46
3	mz, brown-yellow	0.0082	2	4743	1071.78	18.4	13.20	6593	0.04915	0.33	0.3561	0.38	0.05254	0.13	309.3	309.3	307.0	0.94
4	mz, brown-yellow	0.0030	3	4709	1097.19	7.3	13.81	6022	0.04864	0.34	0.3523	0.39	0.05252	0.13	306.2	306.4	308.2	0.95
5	z, pr euh clrls	0.0021	5	991	46.32	3.4	0.21	1929	0.04855	0.33	0.3526	0.15	0.05268	0.26	305.6	306.7	315.1	0.64
6	mz, yellow	0.0014	2	6960	1687.53	7.4	14.50	4069	0.04877	0.33	0.3531	0.39	0.05251	0.15	307.0	307.0	307.5	0.93
7	mz, yellow	0.0025	2	1647	702.46	12.2	28.05	1055	0.04840	0.33	0.3511	0.50	0.05261	0.34	304.7	305.5	312.1	0.74
8	z, lpr incl	0.0078	4	592	29.59	8.0	0.39	1816	0.04933	0.34	0.3581	0.44	0.05264	0.33	310.4	310.8	313.5	0.67
191-2	*Casal Vasco granite (deformed granitoid sample with a penetrative D_3 related foliation)*																	
9	z, lpr	0.0037	2	735	34.48	2.5	0.16	3504	0.04944	0.34	0.3589	0.42	0.05265	0.20	311.1	311.4	313.9	0.88
10	z, lpr incl	0.0045	2	809	37.47	2.9	0.16	3842	0.04876	0.33	0.3541	0.41	0.05267	0.19	306.9	307.8	314.6	0.89
11	z, frags of lpr	0.0024	3	799	38.32	4.5	0.31	1327	0.04829	0.36	0.3516	0.52	0.05281	0.34	304.0	306.0	320.8	0.76
12	z, round	0.0014	1	470	21.98	1.7	0.16	1198	0.04935	0.53	0.3581	0.80	0.05262	0.66	310.5	310.8	312.6	0.57
13	mz, yellow round	0.0038	1	8450	1202.51	8.5	7.17	11721	0.04928	0.35	0.3573	0.39	0.05258	0.12	310.1	310.2	310.9	0.95
14	mz, clrls round	0.0083	1	8186	1377.00	13.8	9.06	15419	0.04938	0.35	0.3573	0.39	0.05247	0.12	310.7	310.2	306.1	0.95
154-14	*Junqueira granite (slightly deformed granite sample with a weak tectonic fabric)*																	
15	mz, clrls	0.0024	2	3364	1163.75	6.5	22.20	3891	0.04893	0.33	0.3538	0.40	0.05244	0.16	307.9	307.5	304.5	0.92
16	mz, euh yellow	0.0015	3	5283	1559.29	4.1	18.40	6065	0.04907	0.35	0.3548	0.40	0.05245	0.15	308.8	308.3	305.0	0.93
17	mz, euh clrls	0.0013	3	3214	2308.43	28.8	23.85	890	0.04895	0.34	0.3543	0.55	0.05250	0.39	308.0	307.9	307.1	0.71

[a] Clrls=colourless, euh=euhedral, frags=fragments, incl=inclusions, lpr=long prismatic, mz=monazite, pr=prisms, spr=short prismatic, z=zircon.
[b] Calculated on the basis of radiogenic $^{208}Pb/^{206}Pb$ ratios, assuming concordancy.
[c] Corrected for fractionation and spike.
[d] Corrected for fractionation, spike, blank and common lead (Stacey and Kramers, 1975).
[e] Corrected for initial Th disequilibrium, using an estimated Th/U ratio of 4 for the melt.

Table 4
U–Pb isotopic data on zircon and monazite from late- to post-D_3 granitoids

Sample	Fraction (crystal habit)	Weight (mg)	U (ppm)	Pb* (ppm)	$^{206}Pb/^{204}Pb$ (2σ)	$^{206}Pb^*/^{238}U$ (2σ, %)	$^{207}Pb^*/^{235}U$ (2σ, %)	$^{207}Pb^*/^{206}Pb^*$ (2σ, %)	Age (Ma) ^{238}U (2σ)	Age (Ma) $^{206}Pb^*/^{235}U$ (2σ)	Age (Ma) $^{207}Pb^*/^{206}Pb^*$ (2σ)
39B	*Cota–Viseu undeformed coarse porphyritic biotite granite*										
	A (z, spr)	0.53	783.0	29.5	1760 (1.91)	0.03902 (0.16)	0.28208 (0.30)	0.05243 (0.14)	246.7 (0.4)	252.3 (0.7)	304 (3)
	B (z, flat pr)	0.67	1866.2	74.9	1703 (2.36)	0.04230 (0.13)	0.30590 (0.30)	0.05245 (0.18)	267.1 (0.3)	271.0 (0.7)	305 (4)
	C (z, lpr euh clrls)	1.24	1155.4	47.1	2795 (2.82)	0.04311 (0.11)	0.31175 (0.21)	0.05244 (0.09)	272.1 (0.3)	275.5 (0.5)	305 (2)
	D (z, frags of spr)	0.38	2626.2	112.7	2047 (11.1)	0.04555 (0.07)	0.32937 (0.27)	0.05244 (0.21)	287.1 (0.2)	289.1 (0.7)	305 (5)
	(mz, yellow)	0.10	4563.7	1799.6	1956 (1.91)	0.04863 (3.34)	0.35139 (3.49)	0.05241 (0.16)	306.1 (10.0)	305.8 (9.2)	303 (4)
178-14	*Cota–Viseu undeformed coarse porphyritic biotite granite*										
	A (z, frags of lpr)	0.47	2681.0	109.7	2038 (12.1)	0.04351 (0.09)	0.31485 (0.25)	0.05248 (0.17)	274.6 (0.2)	277.9 (0.6)	306 (4)
	B (z, lpr)	0.38	2615.5	107.3	2516 (10.6)	0.04353 (0.10)	0.31475 (0.22)	0.05244 (0.13)	274.7 (0.3)	277.9 (0.5)	305 (3)
	C (z, spr)	0.32	2614.2	112.2	4630 (8.6)	0.04556 (0.09)	0.33 (0.19)	0.05248 (0.11)	287.2 (0.2)	289.3 (0.5)	306 (3)
	(mz, brown-yellow)	0.22	3332.8	1240.2	2267 (15.1)	0.04857 (1.13)	0.35110 (1.34)	0.052 (0.23)	305.7 (3.4)	305.6 (3.5)	304 (5)

clrls=colourless, euh=euhedral, frags=fragments, lpr=long prismatic, mz=monazite, pr=prisms, spr=short prismatic, z=zircon.

180-10, 191-2 and 154-14 were carried out on a Finnigan MAT 262 mass spectrometer at ETH following the procedure described in Schaltegger and Corfu (1995). Samples 39B and 178-14 were analysed at the CRPG using a Cameca TSN 206 and Finnigan MAT 262 mass spectrometers.

The U–Pb (zircon and monazite) analytical data obtained in this study are presented in Tables 3 and 4.

6. Petrography and geochemistry of studied granites

6.1. Early, syn-D_3 granodiorite–monzogranite suite—Maceira and Casal Vasco granites

The Maceira and Casal Vasco granites crop out in the eastern part of the Viseu area and document the earlier and less voluminous phase of late Variscan magmatic activity. Both massifs show heterogeneous deformation that may result in the development of a gneissic texture. The syn-D_3 tectonic foliation impressed in these granitoids is related to the Juzbado–Penalva do Castelo sinistral shear zone. No evidence for previous tectonic structures was recognized in these lithologies.

Despite their strong deformation fabric, the Maceira and Casal Vasco biotite gneiss–granites still preserve remnants of igneous granitic textures. The main facies range from medium-grained equigranular to K-feldspar porphyritic. The medium-grained equigranular varieties dominate in the Maceira massif, whereas the porphyritic facies are the major lithological type in the Casal Vasco pluton. Mafic microgranular enclaves (MME) are present in both rock units. Mineralogically, the granitoids contain quartz (20–30%), plagioclase (An_{34}–An_{18}) (30–35%), K-feldspar (≈20%), biotite (>10%) as their main constituents and minor amounts of muscovite, apatite, zircon, monazite and opaques. Fibrolite needles and andalusite grains were occasionaly found in some samples of the Casal Vasco granitoids.

The Maceira and Casal Vasco biotite gneiss–granites vary in composition from slightly peraluminous granodiorites to highly peraluminous monzogranites (SiO_2=60–71%; ASI=1.0–1.37). They exhibit rather high Ba and REE contents (Ba=549–2670 ppm; ∑REE=481–681 ppm), significant LREE enrichment

(La_N/Yb_N=34–46) and variable Eu negative anomalies (Eu/Eu*=0.24–0.66). Unlike the syn-D_3 leucogranites, the mineralogical, geochemical and isotopic signatures of the Maceira and Casal Vasco biotite gneiss–granites ($^{87}Sr/^{86}Sr_i \leq 0.710$; $\varepsilon Nd_i = -3.4$ to -6.9) are not easily accounted for by simple partial melting of metasedimentary and/or felsic metaigneous middle crustal lithologies (S-type origin). Although it is possible to propose a derivation from low degrees of dehydration melting of a metasedimentary protolith for these granites, their I–S transitional character can also be explained in terms of anatexis of mixed mafic and felsic lower crustal components and/or hybridization of felsic crustal melts with mantle-derived magmas.

6.2. Syn-D_3 peraluminous leucogranite suite—Junqueira granite

At the presently exposed level, the leucogranites are the major rock type within the group of the syn-D_3 granitoids. This suite is represented in the Viseu area by the two-mica peraluminous granitoids of Junqueira–Serra da Freita (Fig. 2). They show heterogeneous deformation and a NW–SE directed, subvertical, S_3 foliation.

The main facies is a medium-grained equigranular monzogranite consisting of 30% to 36% quartz, 22 to 27% plagioclase (albite–oligoclase), 15% to 20% K-feldspar (microcline), 3% to 10% biotite and muscovite (>8%). Sillimanite, apatite, zircon, monazite and ilmenite are present as accessory phases. The probable crustal origin of these granites is documented by their Al-rich mineralogy. Metasedimentary xenoliths are unevenly distributed throughout the pluton.

Geochemically, the Junqueira granitoids show little compositional variation and a strong peraluminous character (ASI=1.15–1.39). Silica contents range from 71% to 74% SiO_2, Ca and Mg are low (CaO=0.3–0.6%; MgO=0.2–0.6%) and P_2O_5 is high but variable. The major and trace element geochemistry of the Junqueira granitoids is consistent with moderate degrees of partial melting under water-undersaturated conditions of metasedimentary crustal sources (Beetsma, 1995). The published Sr and Nd isotopic data for this type of granitoids ($^{87}Sr/^{86}Sr_i > 0.711$; $\varepsilon Nd_i < -7$) support such a hypothesis (Beetsma, 1995).

6.3. Late to post-D_3 granodiorite–monzogranite suite—Cota–Viseu granite

The different intrusive units of the late- to post-D_3 granodiorite–monzogranite suite occupy most of the central and eastern sectors of the Viseu area (Fig. 2). They form a large, multipulse, composite batholith consisting of volumetrically dominant plutons of biotite monzogranites and two-mica granites and minor satelite bodies of granodiorites, quartz–monzodiorites, monzodiorites and gabbronorites. Small masses and stocks of leucogranites are also observed.

The Cota–Viseu coarse porphyritic biotite monzogranite is the main lithological type within this complex. It occurs as a large, irregularly shaped intrusion, more than 75 km long and 35 km wide and displays discordant relationships with both foliated syn-D_3 granitoids and metasediments of Precambrian–Cambrian to Upper Carboniferous age.

Mineralogically, the Cota–Viseu granite consists of K-feldspar megacrysts up to 8 cm long set in a medium- to coarse-grained groundmass of quartz, plagioclase (An_{15}–An_{32}), K-feldspar (mostly perthitic microcline) and biotite. Accessory minerals include apatite, zircon, monazite, ilmenite and rare xenotime. The presence of abundant mafic microgranular enclaves (MME) within this facies as well as the lobate nature of the contacts between the monzogranite and the small stocks of more mafic rocks (gabbros, monzodiorites, quartz monzodiorites, granodiorites) suggest a significant role for magma mixing processes in their petrogenesis (Azevedo and Nolan, 1998).

Taken together, the different units of the late-post-D_3 granodiorite–monzogranite suite are characterized by a wide compositional range (SiO_2=52–76%; MgO=7.3–0.1%) and I-type high-K calc-alkaline affinities. The least evolved members of the suite are dominantly metaluminous (ASI<1.0), the Cota–Viseu biotite monzogranite is slightly peraluminous (ASI=0.9–1.12) and the more evolved two-mica granites exhibit peraluminous signatures (ASI=1.0–1.22). The existing Rb–Sr and Sm–Nd isotopic data for the different units ($^{87}Sr/^{86}Sr_i$=0.704–0.708; εNd_i=+0.6 to −3.5) appear to support a model involving crustal assimilation and contamination of mantle-derived magmas as well as biotite+plagioclase fractionation under relatively high water pressures (Azevedo and Nolan, 1998).

7. Results of U–Pb age determinations

7.1. Early, syn-D_3 granodiorite–monzogranite suite—Maceira granite

The zircon population of the sample 180-10 from the Maceira granite consists of long prismatic to short prismatic zircon crystals with (211) faces. The selected grains have 550 ppm to 1000 ppm U and are free of any visible inherited cores. Four single-grain zircon fractions (1, 2, 5, 8) are concordant or only slightly discordant and straddle a discordia line intersecting the concordia at 314±5 Ma (Table 3).

The monazite fractions consist of slightly coloured (yellow to brownish) grains containing up to 7000 ppm U. Th/U ratios are highly variable between 7 and 24. Analyses 3, 4, 6 and 7 are analytically concordant and straddle the concordia between 309 and 305 Ma. All monazite data have been corrected for initial ^{230}Th disequilibrium using an estimated Th/U ratio of 4 in the source. The zircon and monazite data suggest that the age of crystallization is older than 309 Ma (oldest monazite grain). The zircon points may be interpreted by a lead loss line passing through zero, but some influence of inherited lead cannot be excluded. We estimate the age of granite crystallization to be represented by the upper intercept of the zircon discordia at 314±5 Ma (Fig. 4). The monazites possibly record protracted growth over some 4 my and/or subordinate degrees of lead loss. Monazite analysis 3 is supposed to be the closest to the actual age of crystallization (^{207}Pb/^{235}U age of 309.3 Ma). The monazite data could alternatively represent post-emplacement growth due to the thermal influence induced by the intrusion of the nearby Casal Vasco granite suite.

7.2. Early, syn-D_3 granodiorite–monzogranite suite—Casal Vasco granite

The zircon population of the Casal Vasco granite (sample 191-2) is very heterogeneous and comprises several subpopulations of different shape, colour and morphology. Fractions 9 and 12 are analytically concordant and consist of two long-prismatic and one rounded grain, respectively. Analyses 10 and 11 both corresponding to long prismatic zircon micro-fractions, are biased by both lead loss and inheritance since they are straddling a discordia line with largely negative lower intercept (−480±610 Ma; Fig. 4). U contents are around 800 ppm for long prismatic zircon grains and 470 ppm for a rounded crystal. Monazites are yellowish and contain around 8000 ppm U. The two analysed monazite grains have similar Th/U ratios of 7 and 9 and yielded an identical ^{207}Pb/^{235}U age of 310.2 Ma. The emplacement of the Casal Vasco granite is perfectly dated at 311±1 Ma by the mean ^{206}Pb/^{238}U age of four zircon and monazite fractions (9, 12, 13, 14). This age is in full agreement with the upper intercept age of 311±2 Ma calculated from a concordia line of all 6 analyses.

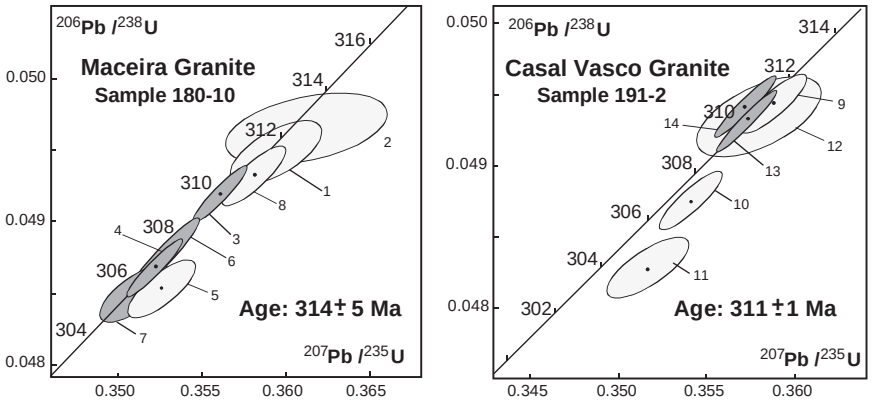

Fig. 4. U–Pb concordia diagrams for zircon and monazite fractions from the syn-D_3 biotite monzogranites. Grey-coloured and light coloured ellipses refer to monazite and zircon, respectively.

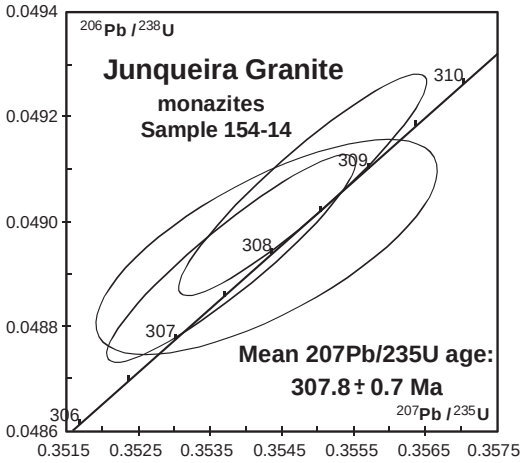

Fig. 5. U–Pb concordia diagrams for monazite fractions from the syn-D_3 Junqueira two-mica granite.

7.3. Syn-D_3 peraluminous leucogranite suite—Junqueira granite

Given the probable crustal origin of the Junqueira–Serra da Freita granite, we envisaged the presence of inherited cores in the zircons and therefore only monazite grains were used for dating purposes. Three yellowish to nearly colourless monazite microfractions of 2–3 grains each were dated, which yielded slightly reversely concordant points (despite the disequilibrium correction of ^{230}Th) at an average ^{207}Pb/^{235}U age of 307.8±0.7 Ma (Table 3, Fig. 5).

As a result of the syn-D_3 tectonic character of the Junqueira–Serra da Freita leucogranites, the 308 Ma U–Pb age can be used to date the D_3 deformation event. Similar ages (≈310 Ma) were obtained in monazites (Chaminé et al., 1998) and micas (Acciaioli et al., 2003) for rocks of adjacent sectors of the CIZ, using and U–Pb and Ar–Ar dating techniques, respectively.

7.4. Late-post-D_3 granodiorite–monzogranite suite—Cota–Viseu granite

Two samples of the Cota–Viseu granite (39B and 178-14) were selected for conventional multi-grain U–Pb analysis of zircon and monazite grains. The analysed zircon fractions of each sample were separated according to the morphology and length/width ratio of the crystals. The four zircon fractions for sample 39B define a discordia (MSWD=2.97) with an upper intercept at 305±4 Ma (Table 4, Fig. 6) whilst the three zircon fractions of sample 178-14 are aligned along a discordia with an upper intercept at 308±8 Ma (MSWD=0.46) (Fig. 6). The monazite fractions of both samples are slightly reversely discordant and yield the same ^{207}Pb/^{235}U age (306±9 Ma and 306±4 Ma, respectively) (Table 4).

Early attempts to date the Cota–Viseu granite using the Rb–Sr whole rock method yielded ages ranging between 282±6 Ma (Pereira, 1991), 308±11 Ma (Silva, 1995) and 315±9 Ma (Azevedo and Nolan, 1998).

In view of the good agreement of the monazite ages obtained in this study for the two samples of the Cota–Viseu granite, the 306 Ma age is interpreted here as the crystallization age of the coarse porphyritic biotite granites. This date is within the

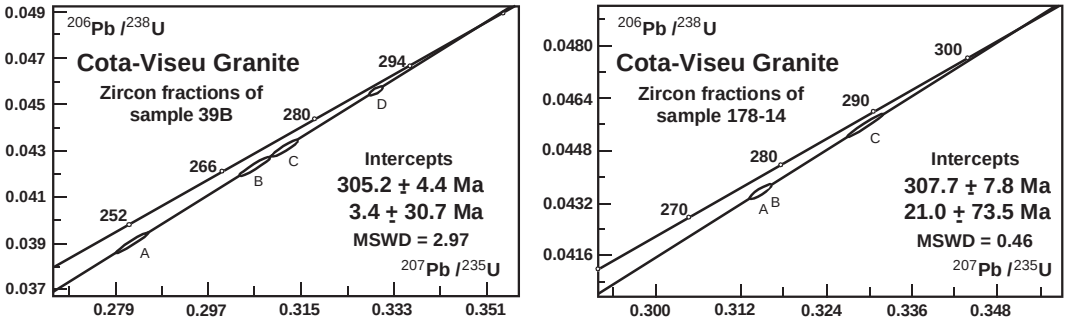

Fig. 6. U–Pb concordia diagrams for zircon fractions from the late-post-D_3 Cota–Viseu coarse porphyritic biotite monzogranite.

maximum and minimum limits suggested by geological constraints and provides relevant information on the timing of the D_3 deformation event. As these granites clearly cross cut the DBSZ shear zone, it is possible to conclude that the operation of this major shearing episode ended before 306 Ma.

8. Discussion and conclusions

The Carboniferous tectono-magmatic evolution of the Viseu area can be summarized in the following way:

a) The migmatites and medium- to high-grade metapelites of the Porto–Viseu Belt record a significant history of high-temperature decompression followed by rapid cooling. Mineral assemblages and reaction textures from rocks of the deepest crustal levels indicate decompression from the kyanite stability field to the sillimanite field, with maximum temperatures of ca. 750 °C (Fig. 3). The existing structural data for the migmatites of the Porto–Viseu antiform suggest a close temporal link between partial melting and the D_2 extensional deformation event. Tectonic exhumation has also lead to the formation of the Upper Carboniferous intramontane limnic basin, either at the end of D_2 crustal extension or in a transitional transtensional regime.
b) The 314–311 Ma Maceira and Casal Vasco granites intruded along a high strain, ENE–WNW trending, sinistral, D_3 shear zone (JPCSZ) that affects the central part of the Viseu area. Considering the possible involvement of a mantle component in the genesis of these melts and their syn-D_3 tectonic character, it may be inferred that the JPCSZ was a major crustal to lithospheric-scale structure, which tapped deep-seated magma chambers. Fluids circulating along the transcurrent fault would have favoured melting of lower crustal lithologies, triggered by heat transfer from mantle-derived magmas.
c) The syntectonic intrusion of the 308 Ma Junqueira–Serra da Freita leucogranites, controlled by the D_3 shear zones, proves that isothermal decompression melting of middle-crustal rock portions continued throughout the D_3 transpressive episode. Although the timing of the HT-LP metamorphic climax in the Viseu area has not been precisely determined, it is unlikely that decompression occurred much prior to the extraction and crystallization of these melts because the crust would tend to cool rapidly during the decompression stage. The 308 Ma U–Pb age of the Junqueira–Serra da Freita leucogranites provides therefore a time constraint for the age of the metamorphic peak which cannot therefore be much older than 308 Ma. This fact implies very fast uplift rates during this transpressional shearing.
d) The emplacement of abundant volumes of syn-D_3 granitoids (314–308 Ma) is interpreted as evidence for continued tectonic exhumation in an essentially transcurrent regime related to ENE–WSW to NW–SE sinistral and NNW–SSE conjugate dextral shear zones. Ductile deformation, exhumation of high-grade rocks and syn-D_3 magmatism are concomitant processes and appear to have occurred at the same time as active erosion and subsidence of the Upper Carboniferous basin was taking place. The D_3 deformation event ends with the inversion of this basin.
e) The next recorded event is the emplacement of the large 306 Ma Cota–Viseu acid–basic association. These granitoids are intrusive in the syn-D_3 plutons, cross-cut the D_3 regional structures and impose contact metamorphism onto the Upper Carboniferous sequence, documenting the end of the operation of the syn-D_3 DBSZ and JPCSZ shearing. The geochemical and isotopic signature of this suite reflects an increasing involvement of mid-crustal sources mixed with asthenospheric material (Beetsma, 1995; Azevedo and Nolan, 1998). Basaltic melts generated within the upwelling asthenosphere may have pond at the crust–mantle boundary supplying heat to an exhuming continental crust, warmed by radioactive decay.

The Carboniferous tectono-magmatic evolution of the Viseu area is interpreted in a scenario of restoration to normal size of a thickened continental lithosphere. Rapid subsidence, deformation and voluminous granite magmatism are short-lived and coeval processes which changed the structure of the orogen within a few million years.

Acknowledgements

J. Leterrier is greatly thanked for U–Pb isotope dating of the Cota–Viseu granite. Technical help during sample preparation and mass spectrometry at ETH Zurich by M.T. Baer, I. Ivanov and A. von Quadt is kindly acknowledged. Thorough reviews and valuable comments by F. Finger, U. Poller and J. Kotkova are greatly appreciated.

This investigation was carried out in the scope of two research projects (PRAXIS 2/2.1/CTA/94 and POCTI/CTA/35630/99), financially supported by the Portuguese Foundation of Science and Technology (FCT).

References

Ábalos, B., Carreras, J., Druguet, E., Escuder Viruete, J., Gómez Pugnaire, M.T., Lorenzo Álvarez, S., Quesada, C., Rodríguez Fernández, L.R., Gil Ibarguchi, J.I., 2002. Variscan and pre-Variscan tectonics. In: Gibbons, W., Moreno, M.T. (Eds.), The geology of Spain. Geological Society, London, pp. 155–183.

Acciaioli, M.H., Santos, J.F., Munhá, J.M., Cordani, U.G., Couto, A., Sousa, P., 2003. Idades Ar–Ar em micas de metapelitos da zona de Espinho: Datação do metamorfismo relacionado com a F3 varisca. IV Congresso Ibérico de Geoquímica e XIII Semana de Geoquímica, Coimbra (Portugal), Abstracts, pp. 161–163.

Azevedo, M.R., Nolan, J., 1998. Hercynian late-post-tectonic granitic rocks from the Fornos de Algodres area (Northern Central, Portugal). Lithos 44, 1–20.

Beetsma, J.J., 1995. The late Proterozoic/Paleozoic and Hercynian crustal evolution of the Iberian Massif, N Portugal. PhD thesis, Vrije University, Netherlands, 223 pp.

Behr, H.J., Hengel, W., Franke, W., Giese, P., Weber, K., 1984. The Variscan belt in central Europe: main structures, geodynamic implications, open questions. Tectonophysics 109, 15–40.

Behrmann, J., Drozdzewski, G., Heinrichs, T., Huch, M., Meyer, W., Oncken, O., 1991. Crustal-scale balanced cross-sections through the Variscan Fold Belt, Germany: the central EGT-segment. Tectonophysics 142, 173–202.

Black, R., Liégeois, J.-P., 1993. Cratons, mobile belts, alkaline rocks and the continental lithospheric mantle: the Pan-African testimony. J. Geol. Soc. (Lond.) 150, 89–98.

Burg, J.-P., Ford, M., 1997. Orogeny through time: an overview. In: Burg, J.P., Ford, M. (Eds.), Orogeny through Time, Special Publication - Geological Society of London, vol. 121, pp. 1–17.

Burg, J.-P., Van Den Driessche, J., Brun, J.-P., 1994. Syn- to post-thickening extension in the Variscan Belt of Western Europe: modes and structural consequences. Géol. Fr. 3, 33–51.

Carrington da Costa, J., 1950. Notícia sobre uma carta geológica do Buçaco de Nery Delgado. Comun. Serv. Geol. Port. (28 pp.).

Chaminé, H.I., Leterrier, J., Fonseca, P., Ribeiro, A., Sousa, M.J.L., 1998. Geocronologia U–Pb em zircões e monazites de rochas ortoderivadas do sector de Espinho—Albergaria-a-Velha. Comun. Inst. Geol. Min. Port. 84 (2), B115–B118.

Dallmeyer, R.D., Martínez Catalán, J.R., Arenas, R., Gil Ibarguchi, J.I., Gutiérrez Alonso, G., Farias, P., Bastida, F., Aller, J., 1997. Diachronous Variscan tectonothermal activity in the NW Iberian Massif: evidence from $^{40}Ar/^{39}Ar$ dating of regional fabrics. Tectonophysics 277, 307–337.

Davies, J.H., Von Blanckenburg, F., 1995. Slab break-off: a model of lithosphere detachment and its test in the magmatism and deformation of collisional orogens. Earth Planet. Sci. Lett. 129, 85–102.

Dias, R., 1994. Regimes de Deformação no Autóctone da ZCI: Importância para a compreensão da Génese do Arco Ibero–Armoricano. PhD thesis, University of Lisbon (Portugal).

Dias, G., Leterrier, J., Mendes, A., Simões, P.P., Bertrand, J.M., 1998. U–Pb zircon and monazite geochronology of post-collisional. Hercynian granitoids from the Central Iberian Zone (Northern Portugal). Lithos 45, 349–369.

Díez Balda, M.A., Vegas, R., Gonzalez Lodeiro, F., 1990. Central Iberian Zone: structure. In: Dallmeyer, R.D., Martinez Garcia, E. (Eds.), Pre-Mesozoic geology of the Iberian Peninsula. Springer Verlag, Berlin, pp. 172–188.

Díez Balda, M.A., Martínez Catalán, J.R., Ayarza Arribas, P., 1995. Syn-collisional extensional collapse parallel to the orogenic trend in a domain of steep tectonics: the Salamanca Detachment Zone (Central Iberian Zone, Spain). J. Struct. Geol. 17, 163–182.

Escuder Viruete, J., Arenas, R., Martínez Catalán, J.R., 1994. Tectonothermal evolution associated with Variscan crustal extension in the Tormes Gneiss Dome (NW Salamanca, Iberian Massif, Spain). Tectonophysics 238, 117–138.

Farias, P., Gallastegui, G., González-Lodeiro, F., Marquínez, J., Martín Parra, L.M., Martínez Catalán, J.R., de Pablo Maciá, J.G., Rodríguez Fernández, L.R., 1987. Aportaciones al conocimiento de la litoestratigrafía y estructura de Galicia Central. Mem. Fac. Ciênc. Univ. Porto 1, 411–431.

Ferreira, N., Iglesias Ponce de Léon, M., Noronha, F., Ribeiro, A., Ribeiro, M.L., 1987. Granitóides da Zona Centro Ibérica e seu enquadramento geodinâmico. In: Bea, F., Carnicero, A., Gonzalo, J.C., López Plaza, M., Rodriguez Alonso, M.D. (Eds.), Geologia de los granitoides e rocas asociadas del Macizo Hespérico. Editorial Rueda, Madrid, pp. 37–51.

Finger, F., Roberts, M.P., Haunschmid, B., Schermaier, A., Steyrer, H.P., 1997. Variscan granitoids of central Europe: their typology, potential sources and tectonothermal relation. Mineral. Petrol. 61, 67–96.

Holdaway, M.J., 1971. Stability of andalusite and the aluminum silicate phase diagram. Am. J. Sci. 271, 97–131.

Iglesias, M., Ribeiro, A., 1981. La zone de cisaillement ductile de Juzbado (Salamanca)–Penalva do Castelo (Viseu): Un linéament ancien reactivé pendant l'orogenese Hercynienne? Comun. Serv. Geol. Port. 67 (1), 89–93.

Julivert, M., Fontbote, J.M., Ribeiro, A. and Conde, L., 1972. Mapa Tectónico de la Península Ibérica y Baleares, E. 1: 1.000.000. Inst. Geol. Min. Esp. Madr.

Julivert, M., Fontbote, J.M., Ribeiro, A., Conde, L., 1974. Mapa Tectónico de la Península Ibérica y Baleares (Memoria). Inst. Geol. Min. Esp. Madr. (113 pp.).

Krogh, T.E., 1973. A low contamination method for the hydrothermal decomposition of zircon and extraction of U–Pb for isotopic age determination. Geochim. Cosmochim. Acta 37, 485–494.

Krogh, T.E., 1982. Improved accuracy of U–Pb zincon ages by the creation of more concordant systems using an air abrasion technique. Geochim. Cosmochim. Acta 46, 637–649.

Luth, W.C., Jahns, R.H., Tuttle, O.F., 1964. The granite system at pressures of 4 to 10 kilobars. J. Geophys. Res. 69, 759–773.

Noronha, F., Ramos, J.M.F., Rebelo, J.A., Ribeiro, A., Ribeiro, M.L., 1981. Essai de corrélation des phases de déformation hercyniennes dans le nord-ouest Péninsulaire. Leidse Geol. Meded. 52, 87–91.

Pereira, A.J.S.C., 1991. Transferências de calor e ascensão crustal no segmento Tondela-Oliveira do Hospital (Portugal Central) após a implantação dos granitos hercínicos sin a tardi-orogénicos. PhD thesis, University of Coimbra, Portugal, 182 pp.

Pinto, M.S., Casquet, C., Ibarrola, E., Corretgé, L.G., Portugal Ferreira, M., 1987. Síntese geocronológica dos granitóides do Maciço Hespérico. In: Bea, F., Carnicero, A., Gonzalo, J.C., López Plaza, M., Rodriguez Alonso, M.D. (Eds.), Geologia de los granitoides e rocas asociadas del Macizo Hespérico. Editorial Rueda, Madrid, pp. 69–86.

Priem, H.N., Schermerhorn, L.J.G., Boelrijk, N.A.I.M., Hebeda, E.H., 1984. Rb–Sr geocronology of Variscan granitoids in the tin–tungsten province of northern Portugal: a progress report. Terra Cogn. 4, 212–213.

Reavy, R.J., 1987. An investigation into the controls of granite plutonism in the Serra da Freita region, northern Portugal. PhD thesis, University of St. Andrews.

Rey, P., Burg, J.-P., Casey, M., 1997. The Scandinavian Caledonides and their relationship to the Variscan Belt. In: Burg, J.P., Ford, M. (Eds.), Orogeny through Time, Special Publication - Geological Society of London, vol. 121, pp. 179–200.

Ribeiro, A., Pereira, E., Severo, L., 1980. Análise da deformação na zona de cisalhamento Porto–Tomar na transversal de Oliveira de Azeméis. Comun. Serv. Geol. Port. 66, 33–48.

Ribeiro, A., Pereira, E., Dias, R., 1990. Central-Iberian Zone. Allochthonous sequences. Structure in the Northwest of the Iberian Peninsula. In: Dallmeyer, R.D., Martinez Garcia, E. (Eds.), Pre-Mesozoic geology of the Iberian Peninsula. Springer Verlag, Berlin, pp. 220–236.

Rottura, A., Del Moro, A., Pinarelli, M., Petrini, R., Caggianelli, A., Bargossi, J.M., Piccarreta, G., 1991. Relationships between intermediate and acidic rocks in orogenic granitoid suites: petrological, geochemical and isotopic (Sr, Nd, Pb) data from Capo Vaticano (southern Calabria, Italy). Chem. Geol. 92, 153–176.

Schaltegger, U., Corfu, F., 1995. Late Variscan "basin and range" magmatism and tectonics in the Central Alps: evidence from U–Pb geochronology. Geodin. Acta 8, 82–98.

Schulmann, K., Schaltegger, U., Jezek, J., Thompson, A.B., Edel, J.B., 2002. Rapid burial and exhumation during orogeny: thickening and synconvergent exhumation of thermally weakened and thinned crust (Variscan orogen in Western Europe). Am. J. Sci. 302, 856–879.

Shaw, A., 1991. The petrogenesis of Hercynian granites, French Massif Central. Unpublished PhD thesis, University of London, UK, 285 pp.

Silva, M.M.V.G., 1995. Mineralogia, petrologia e geoquímica de encraves de rochas graníticas de algumas regiões portuguesas. PhD thesis, University of Coimbra, Portugal, 288 pp.

Stacey, J.S., Kramers, J.D., 1975. Approximation of terrestrial lead isotope evolution by a two-stage model. Earth Planet. Sci. Lett. 26, 207–221.

Sylvester, P.J., 1998. Post-collisional strongly peraluminous granites. Lithos 45, 29–44.

Teixeira, C., 1954. Os conglomerados do Complexo Xisto-Grauváquico ante-silúrico. Comun. Soc. Geol. Porto. 35, 33–49.

Thirlwall, M.F., 1991. Long-term reproducibility of multicollector Sr and Nd isotope ratio analysis. Chem. Geol. 94, 85–104.

Thompson, A.B., Connoly, J.A.D., 1995. Melting of the continental crust: some thermal and petrologic constraints on anatexis in continental collision zones and other tectonic settings. J. Geophys. Res. 100, 15565–15579.

Valle Aguado, B., 1992. Geología estructural de la Zona de Cisalla de Porto-Tomar en la región de Oliveira de Azeméis-Serra de Arada (Norte de Portugal). PhD thesis, University of Salamanca, Spain, 254 pp.

Valle Aguado, B., Arenas, R., Martínez Catalán, J.R., 1993. Evolución metamórfica hercínica en la región de la Serra de Arada (Norte de Portugal). Comun. Inst. Geol. Min. Port. 79, 41–61.

Valle Aguado, B., Martínez Catalán, J.R., Azevedo, M.R., 2000. Structure of the western termination of the Juzbado–Penalva do Castelo Shear Zone (Western Iberian Massif). Variscan–Appalachian dynamics: the building of the Upper Paleozoic basement, A Coruña, Spain, Program and Abstracts. Basement Tectonics 15, pp. 287–291.

Valverde Vaquero, P., 1997. An integrated field, geochemical and U–Pb geochronological study of the SW Hermitage Flexure (Newfoundland Appalachians, Canada) and The Sierra de Guadarrama (Iberian Massif, Central Spain): a contribution to the understanding of the geological evolution of circum-Atlantic peri-Gondwana. PhD thesis, Memorial University of Newfoundland, St. John's.

Watkins, P.J., Nolan, J., 1990. Determination of rare-earth elements, scandium yttrium and hafnium in 32 geochemical reference materials using inductively coupled plasma-atomic emission spectrometry. Geostand. Newsl. 14 (1), 11–20.

Watkins, P.J., Nolan, J., 1992. Determination of rare-earth elements, yttrium, scandium and hafnium using cation-exchange separation and inductively coupled plasma-atomic emission spectrometry. Chem. Geol. 95, 131–139.

Wickham, S.M., Oxburgh, E.R., 1987. Low-pressure regional metamorphism in the Pyrénées and its implications for the thermal evolution of rifted continental crust. Philos. Trans. R. Soc. Lond., A 321, 219–242.

Yardley, B.W.D., 1989. An introduction to metamorphic petrology. Longman Group UK, Essex. 248 pp.